ADVANCED FUNCTIONAL MATERIALS
www.afm-journal.de

A Tailorable Family of Elastomeric-to-Rigid, 3D Printable, Interbonding Polymer Networks

Qing Zhou, Frank Gardea, Zhen Sang, Seunghyun Lee, Matt Pharr, and Svetlana A. Sukhishvili**

Soft materials with widely tailorable mechanical properties throughout the material's volume can shape the future of soft robotics and wearable electronics, impacting both consumer and defense sectors. Herein, a platform of 3D printable soft polymer networks with unprecedented tunability of stiffness of nearly three orders of magnitude (MPa to GPa) and an inherent capability to interbond is reported. The materials are based on dynamic covalent polymer networks with variable density of crosslinkers attached to prepolymer backbones via a temperature-reversible Diels–Alder (DA) reaction. Inherent flexibility of the prepolymer chains and controllable crosslinking density enable 3D printed networks with glass transition temperatures ranging from just a few degrees to several tens of degrees Celsius. Materials with an elastomeric network demonstrate a fast and spontaneous self-healing behavior at room temperature both in air and under water—a behavior difficult to achieve with other crosslinked materials. Reversible dissociation of DA networks at temperatures exceeding ≈120 °C allows for reprintability, while control of the stereochemistry of DA attachments enables reprogrammable shape memory behavior. The introduced platform addresses current major challenges including control of polymer interbonding, enhanced mechanical performance of printed parts, and reprocessability of 3D-printed crosslinked materials in the absence of solvent.

1. Introduction

Biological soft materials, such as skin, tendons, fibrous tissues, and blood vessels, are hierarchically integrated at multiple scales, exhibit seamless bonding between dissimilar tissues of different stiffness, and are intrinsically healing.[1] However, mimicking these desirable behaviors with synthetic materials remains challenging.[2] Conventional molding and subtractive manufacturing techniques fall short in achieving local control of material properties. While advanced gradient soft materials can be created using spin-coating or feed mixing materials with different compositions,[3] it was not until the advent of 3D printing that the promise of controlling material composition and properties in all three dimensions opened up.[4] Currently, multimaterial objects of complex shapes can be fabricated using advanced printing techniques, such as suspended layer additive manufacturing, which employs complex liquid ink formulations.[5] The fluidity of the inks is achieved by the addition of solvents and/or liquid monomers whose in situ or post polymerization helps to achieve good interlayer adhesion during layer-by-layer printing.[5] In contrast, good interlayer bonding is much more difficult to achieve with simpler 3D printing techniques, such as fused deposition modeling (FDM).[6] The FDM technique relies on the use of filaments of thermoplastic polymers or their nanocomposites and is the simplest and the most cost-effective by comparison with other 3D printing techniques.[7] Nevertheless, high viscosity of the solvent-free resins leads to poor interlayer adhesion during layer-by-layer deposition, resulting in a significantly lower mechanical strength of the FDM-printed objects as compared to those fabricated using conventional molding techniques. One approach to improving the interlayer strength of printed objects involves photopolymerizable resins;[4a] however, it produces non-reprocessible, permanently crosslinked materials. Yet another approach, based on photothermally active inorganic additives, requires post-treatment and can negatively affect material properties and reprocessability.[8]

Dynamic covalent polymer networks provide an appealing solution to weak interlayer adhesion, while simultaneously enabling reprocessability of 3D-printed materials. Reactions specifically suitable for applications in printable materials are those based on the Diels–Alder (DA) reaction—a cycloaddition reaction of a conjugated diene to an alkene. Because of its "click" characteristics and absence of side products, this reaction has

Q. Zhou, Z. Sang, Prof. S. A. Sukhishvili
Department of Materials Science and Engineering
Texas A&M University
College Station, TX 77843, USA
E-mail: svetlana@tamu.edu
Dr. F. Gardea
U.S. Army Combat Capabilities Development Command
Army Research Laboratory South
Vehicle Technology Directorate
College Station, TX 77843, USA
E-mail: frank.gardea4.civ@mail.mil
S. Lee, Prof. M. Pharr
Department of Mechanical Engineering
Texas A&M University
College Station, TX 77843, USA
The ORCID identification number(s) for the author(s) of this article can be found under https://doi.org/10.1002/adfm.202002374.

DOI: 10.1002/adfm.202002374

been widely used in macromolecular synthesis.[9] A unique feature of several DA reactions,[10] including the one that involves maleimide and furan moieties, is their thermal reversibility. These moieties covalently attach to one another at ambient and mildly high temperatures and break apart when temperature exceeds ≈110 °C.[9a,11] Reversibility of this reaction has been used to create a range of polymer materials with unique characteristics.[11a,12] The first and most striking feature of these materials is that while they are stabilized by a covalently bonded network, and thus are similar to conventional thermosets at ambient conditions, they can be remolded by heating to a high temperature that destroys the network of covalent bonds, followed by cooling to ambient temperature.[13] Another feature of the DA-based polymers (DAPs) is their capability to heal via a similar process of heating-induced dissociation of covalent bonds. The energy required to break C—C bonds in the DA adducts is much lower than that needed for dissociation of conventional single C—C bonds, and therefore crack propagation is likely to occur via decoupling of DA adducts.[9b,12a,14] When heated, furan and maleimide moieties are released via the reversible DA reaction, and therefore are available for mending the damaged material interfaces.[12a,f] As such, the cracks and fractures are restored to a certain degree via reformation of DA from the furan and maleimide moieties available at the crack site. This process can be used to repair damage in polymer networks and can be repeated several times without special surface treatment or the aid of monomers and/or catalysts.[12a,15] However, a high efficiency of healing has not yet been achieved with DA materials at room temperature.

Recently, the advantages of DA reactions were leveraged to achieve 3D printable networks. Reversible dissociation of covalent bonds at increased temperature allows the crosslinking network to dissociate and form during extrusion, enabling printability of covalent networks in a manner similar to conventional thermoplastics. Through DA reactions, layers of the deposited materials can covalently crosslink "on-the-fly," resulting in mechanical strength of printed objects comparable to that of their bulk-processed counterparts. Currently, the only reported printable DA networks (also termed DA reversible thermosets, DART)[16] involve low-molecular furans and maleimide moieties with multiple functional groups. Such approach leaves little room for tuning materials properties, leading to densely crosslinked rigid materials. Creating a versatile system that enables 3D printing of covalently crosslinked polymers with a wide range of mechanical properties has therefore remained challenging. Even for a large family of materials of non-DA chemistry, printing has been largely limited to either constructing permanently crosslinked networks or to the use of block copolymers with high glass transition temperatures, such as in thermoplastic polyurethane. In the latter materials, formation of a physical network of microphase-separated block copolymers at ambient temperature and melting of such a network at an elevated temperature enables materials reprocessability.[17]

Here, we explore a reversible covalent DA reaction to introduce a family of reprintable covalently crosslinked polymer networks. By varying the concentration of a bismaleimide crosslinker, polymer networks with tunable Young's moduli ranging over almost three orders of magnitude were achieved. Low-modulus DAPs exhibit fast room-temperature healing in various environments, including ambient air and/or water, without the need to apply external stimuli. At the same time, high-modulus DAPs demonstrate load-bearing properties. From the 3D printability perspective, a significant advantage of the developed platform is that materials with drastically different mechanical properties can be fabricated using the same constant processing parameters. Importantly, the low viscosity of the printed components during deposition and chemical reactivity of the crosslinker collectively ensure strong interbonding between printed layers with various mechanical gradients, thereby facilitating the facile fabrication of 3D-printed materials with robust interfacial adhesion. Moreover, taking advantage of different strengths of *endo* and the *exo* adducts of DA reactions, we have demonstrated reprogramming of the shape-memory effects with 3D-printed objects via temperature-induced *endo*-to-*exo* rearrangement of the dynamic covalent network.

2. Results and Discussion

Figure 1 illustrates the main features of 3D printing of DAP networks. The resin consists of a mixture of oligomeric linear prepolymer and a bismaleimide (BMI) crosslinker (see the Experimental Section and Figures S1–S3, Supporting Information, for details of synthesis and characterization). The linear prepolymer was terminated with furan groups as shown in Figure S1 (Supporting Information), with an average number of 19 repeating units, as determined by gel permeation chromatography (GPC) (Figure S2a, Supporting Information). Importantly, the prepolymer remained in liquid form over a wide range of temperatures above its glass transition temperature, T_g, of −10.6 °C (Figure S2b, Supporting Information). This feature enabled easy solvent-free handling of the resin synthesis. The material used for 3D printing was then prepared by addition of different amounts of BMI crosslinker, whose ends covalently attached to the furan groups of the prepolymer via a thermally reversible DA reaction between the furan and maleimide groups. The DA polymers containing different amounts of added BMI, and thus different mole ratios of maleimide-to-furan groups Φ_{BMI}, are abbreviated as DAP Φ_{BMI}, where Φ_{BMI} is varied from 0.4 to 0.7. In all cases, Φ_{BMI} was less than unity (i.e., the amount of added crosslinker was a limiting reagent) and DAPs of all compositions contained excess of furan groups. The dynamic nature of the DA reaction (Figure 1a, reversible DA reaction) allowed the network to dissociate to individual BMI and prepolymer components when exposed to temperatures above the dissociation temperature (T_D) and reform below that temperature. Figure S3 (Supporting Information) shows schematics of reversible crosslinking between the linear prepolymer and the BMI crosslinker. Figure 1b shows, with an example of DAP 0.4, two clearly observed thermal transitions in these materials: one at ≈7 °C, corresponding to the glass transition temperature of DAP 0.4, and an endothermic peak at ≈119 °C, reflecting the dissociation of DA adducts via retro DA reaction when the temperature exceeded T_D. The occurrence of dissociation of DA adducts at increased temperature is due to the exothermic nature of the DA addition.[18] Importantly, because of the choice of oligomeric, low-glass-transition

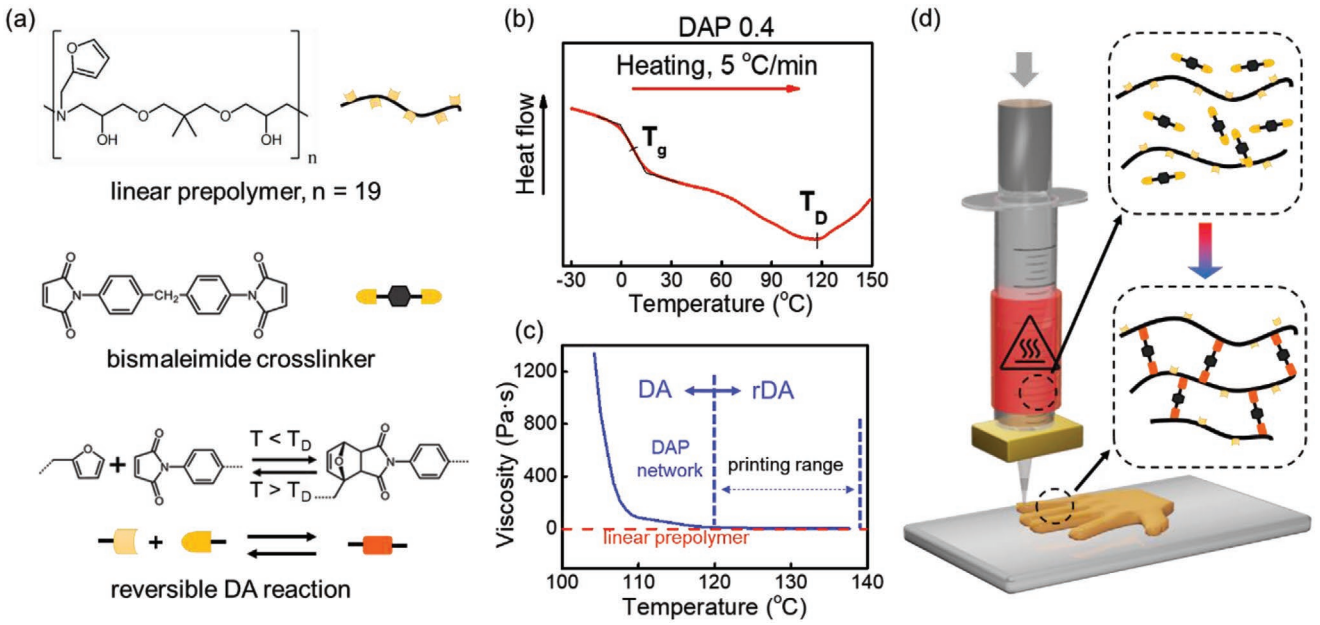

Figure 1. a) Chemical structures of the linear prepolymer and the bismaleimide crosslinker, along with a schematic of the thermally reversible DA reaction between furan and maleimide groups; b) DSC analysis of DAP 0.4 showing T_g and T_D, of 7 and 119 °C, respectively; c) viscosity of the DAP 0.4 and the linear prepolymer as a function of temperature, showing an increase below 120 °C and a sharp increase below 108 °C during cooling at a rate of 5 °C min^{-1}; d) 3D printing process of DAPs extruded through a heated syringe/nozzle above T_D and deposited on a substrate to reform the network upon convective cooling to room temperature.

precursor polymers for this study, polymer networks dissociated to low-viscosity liquids at temperatures exceeding T_D. This is illustrated in Figure 1c by a sharp transition of DAP 0.4 from a covalently crosslinked network to a liquid with a relatively low viscosity of 7 Pa s. This value of viscosity of the dissociated network is similar to that of the original linear prepolymer (3.5 Pa s) at 120 °C. When cooled below 120 °C, the viscosity sharply increased, indicating reformation of the dynamic network. The reversible transition from a reactive liquid to a solid material can be conveniently used in the 3D printing process known as liquid deposition modeling (LDM), in analogy with FDM.[8] In our case, the liquid resin was also reactive and its fast solidification enabled seaming deposition of material and fabrication of parts/objects that retain their shape without the need for postcuring. Figure 1d schematically illustrates the printing process; the DAP materials are extruded through a heated nozzle where they dissociate to the initial prepolymer and crosslinker components. The material is then easily deposited in a layer-by-layer manner to form a 3D object. Though the furan-maleimide reaction is reversible and repeatable in the vicinity of the DA transition,[9a,19] side reactions, such as ring-opening of furan and homopolymerization of maleimide, can occur at significantly higher temperatures,[16,20] which can compromise reprocessability of the DAP materials. Therefore, it was important to keep the temperature below 140 °C during LDM printing. Note that the formation of the crosslinking network was sufficiently fast and was able to pace up with the printing speed. Specifically, we found that the dissociated DAPs were able to solidify in a few seconds after the temperature dropped below T_D. This behavior is due to the large temperature gradient experienced by the material (from 120 °C at the nozzle to room temperature at the substrate/base plate) leading to a rapid increase in viscosity, as observed in Figure 1c. This solidification/dissociation behavior was further studied in rheological experiments in which the response of DAP to an oscillatory shear stress was explored within a temperature range of 70–120 °C with the heating and cooling occurring at the rate of 2.5 °C min^{-1}. Figure S4 (Supporting Information) shows an example of such an approach. During heating/cooling cycles of DAP 0.4, a crossover between the storage modulus (G') and loss modulus (G'') occurred at ≈96 ± 3 °C (98 °C upon heating and 93 °C upon cooling), reflecting dissociation/reformation of the polymer network.[21] These data on mechanical and thermal behavior of DAP networks indicate that DA and retro DA reactions occurred at the time scale comparable or faster than the time scale associated with the 2.5 °C min^{-1} heating/cooling in the rheological experiments.

To further support this conclusion, the degree of conversion of DA reaction after the bulk material was cooled from 120 °C to room temperature was explored. Figure S5c,d (Supporting Information) shows the ^{13}C NMR spectra of the DAP 0.4 and DAP 0.6 recorded 1 h after the polymers were cooled to room temperature. When compared to the spectra of the linear prepolymer and BMI crosslinker (Figure S5a,b, Supporting Information), the chemical shifts at 80 and 176 ppm indicated the newly formed DA bonds. The absence of the chemical shift at 172 ppm suggested full consumption of the BMI crosslinker. Note that prior work on moldable DAP networks reported partially completed DA attachments. For example, the conversion of only 70% of furan groups was achieved with DAPs containing twofold excess of maleimide groups after incubation at room temperature for 24 h.[22] Thus, we believe that the fast and complete DA reaction that lies at the heart of such material behavior is unique in this work. The most important

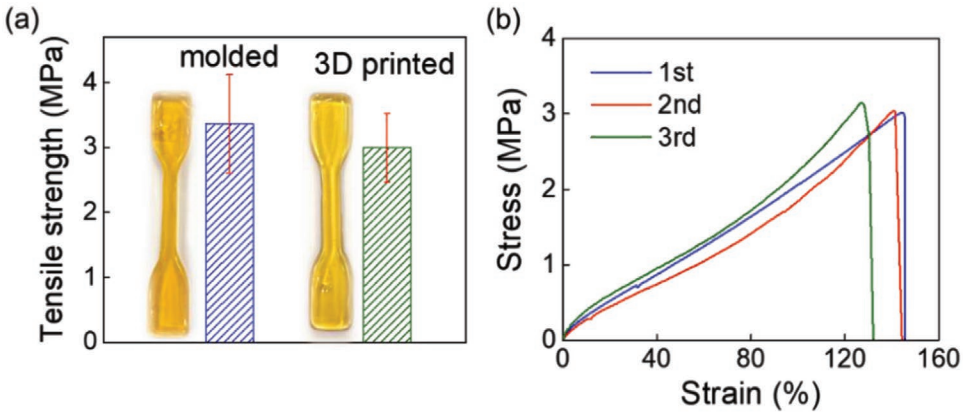

Figure 2. a) 3D-printed and cast-molded DAP 0.4 networks showing similar tensile strength; b) stress–strain curves of the first-time printed (first) and reprinted (second and third) DAP 0.4 specimens, indicating materials reprintability and robust mechanical performance.

factor contributing to this behavior is intrinsic flexibility of the prepolymer backbone, which was a liquid with T_g = –10.6 °C. The rapid crosslinking DA reaction is likely further aided by the presence of the pendant hydroxyl group in the prepolymer chain, which introduced additional polarity to the BMI/prepolymer melts.[23]

A fast DA reaction leads to rapid formation of covalent bonds between the layers of deposited material during 3D printing. As a result, the printed DAPs showed mechanical strength comparable to that of cast molded samples (3.1 ± 0.5 and 3.3 ± 0.7 MPa in tensile strength for 3D-printed and cast-molded specimens, respectively) (**Figure 2**a). The uniformity of the printed materials was also assisted by the fluidity of the resin and its ability to easily flow within a temperature range between 120 and 96 °C, filling the gaps and voids that are commonly seen in conventional FDM-printed materials.[16,24] It is worth noting that the 3D-printed DAP networks could be directly reused for subsequent printing without additional pretreatment or addition of catalysts, such as those required in reversible networks based on transesterification reactions.[25] Figure 2b shows the stress–strain curves of first-time printed (first) and reprinted (second and third) DAP 0.4 specimens. It is observed that the mechanical performance (elastic modulus, tensile strength) was not significantly affected by the repeated printing of the material, pointing to the robustness of mechanical performance of these materials during three printing cycles.

While Figures 1 and 2 show the data for a polymer network with constant crosslinking density, the proposed approach can also be used to generate a family of DAPs with widely varied mechanical properties, achieved via the control of the maleimide-to-furan ratio Φ_{BMI}. **Figure 3**a shows that as the crosslinking density of the network increased upon varying Φ_{BMI} from 0.4 to 0.7, the glass transition temperature of the DAPs increased from 7 to 40 °C. Based on the full conversion of maleimide functional groups, the polymer contour length between crosslinks was estimated as ≈16 and ≈8 nm for DAP 0.4 and DAP 0.7, respectively. To understand the relationship between T_g and the density of crosslinks in DAP networks, we used the following semiempirical equation which was previously developed for crosslinked epoxy materials: $T_g = K_1 \log K_2 \rho$, where ρ is the volumetric crosslinking density (see Table S1, Supporting Information), and K_1 and K_2 are semiempirical constants associated with the restraints to the chain mobility around the crosslinks and the rigidity of polymer chains between crosslinks, respectively.[26] The volumetric crosslinking density was calculated as $\rho = d/M_c$, where d is the density of DAP (≈1 g cm^{-3}), and M_c is the average molecular weight between links. Here, Figure 3b shows that T_g scaled linearly with the logarithm of the crosslinking density of DAP networks, yielding values for K_1 and $\log K_2$ (172 and 3.1, respectively), which were close to those reported for the diamine-cured epoxy resins ($K_1 \approx 200$ and $\log K_2 \approx 3$).[26] Figure 3a also illustrates that regardless of the crosslinking density and T_g of the network materials, the temperature related to the DA reaction (T_D, determined from differential scanning calorimetry (DSC)) remained constant for all DAP materials. This result indicates the robustness of the underlying DA crosslinking of DAP networks and enables the decoupling of processing parameters from the material properties. In other words, all of the polymer networks based on this material system, ranging from elastomeric to rigid, could be conveniently printed using the same printing parameters.

The broad range of T_g leads to a wide range of material mechanical behaviors, with the resultant materials designed to be either soft elastomers or rigid plastics. DAP 0.4 and DAP 0.5 networks behaved as typical elastomers that can undergo large recoverable elastic deformation. As an example, Figure S6 (Supporting Information) shows DAP 0.4 under cyclic tensile loading with a large fully recoverable strain of ≈50%. The tensile strain at break of DAP 0.4 and DAP 0.5 was as high as 140% and 130%, respectively (Figure 3c). At the same time, DAPs with larger content of the crosslinker (DAP 0.6 and DAP 0.7) behaved as brittle materials. This behavior is also demonstrated by the inset images of Figure 3c along with the schematics showing DAPs with lower and higher crosslinking density. Correspondingly, the Young's modulus (E) of DAP materials can be tuned over almost three orders of magnitude from 8.4 MPa to 1.2 GPa (Figure 3d). The tensile strength can be varied between 3 and 30 MPa (Figure 3d).

We next explored the capability of a set of DAP networks with different crosslink densities and widely varied mechanical properties in creating robust 3D printed complex materials with mechanically mismatched interfaces. To that end, a layered heterogeneous object composed of three regions of

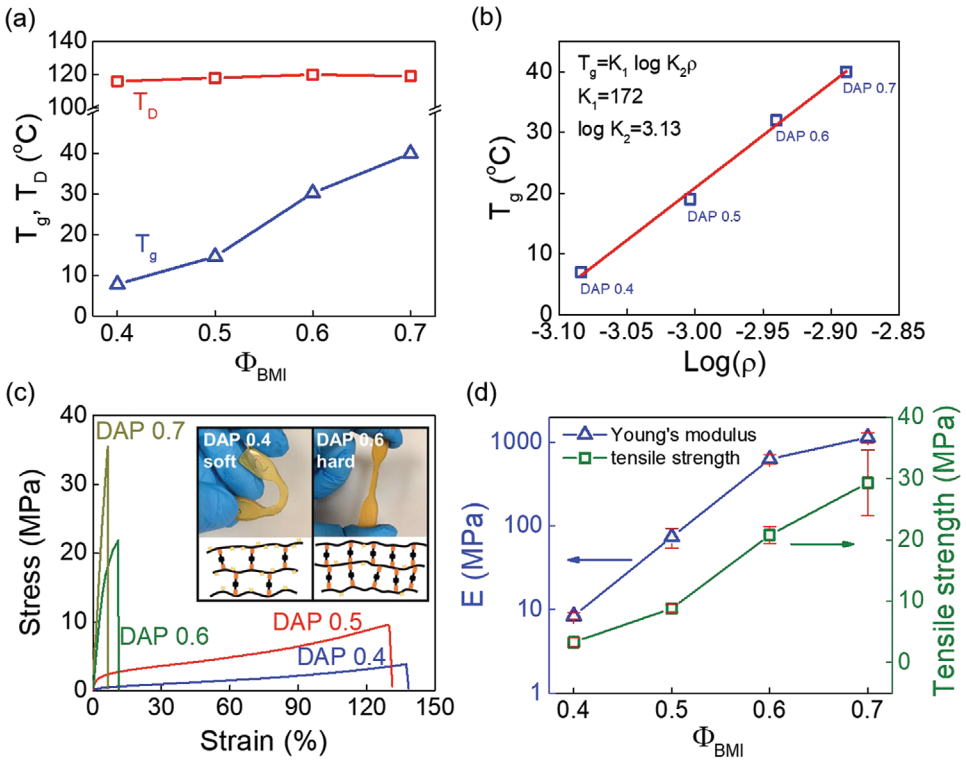

Figure 3. Tunable mechanical properties of DAP networks: a) an increase in T_g of DAPs with Φ_{BMI} = 0.4, 0.5, 0.6, and 0.7 with T_D remaining constant; b) relationship between T_g and crosslinking density, ρ; c) stress–strain curves during tensile testing of DAPs of different crosslinking density; and d) Young's modulus and tensile strength of cast-molded DAP specimens with Φ_{BMI} = 0.4, 0.5, 0.6, and 0.7 (testing conducted at 24 °C).

materials with varied strength and modulus (**Figure 4**a) was designed and manufactured from a single print using multiple syringe extruders, each with a respective DAP. The top layer of the object was constructed with soft elastomeric DAP 0.4 ($E \approx 8$ MPa) and the bottom layer was constructed with hard rigid DAP 0.6 layer ($E \approx 600$ MPa) (Table S1, Supporting Information). The bottom and top layers were separated by a joint middle layer made of DAP 0.5, which was also an elastomer but with an intermediate Young's modulus ($E \approx 70$ MPa). The constructed object (Figure 4b) was tested in uniaxial tension by applying force at the two ends of the rigid layer. The geometric design of the object was guided by the requirement of uniform stress distribution within the material (see the Supporting Information for the geometry design of the heterogeneous object). Upon tensile extension, the construct fractured at the center of the softest layer, away from the joint region, suggesting strong interbonding between the layers of material with mismatched mechanical strength and modulus (Figure 4c). This result favorably compares with generally weak bonding and failures caused by stress concentration at the mechanically mismatched interfaces.[27] Specifically, conventional FDM-printed materials usually suffer from weak interlayer adhesion in the deposition direction due to lack of effective bonding between printed layers.[16,24] In our experiments, the interlayer bonding was strongly aided by the DA-assisted chemical reaction, which ensured interfacial strength and avoided stress concentration at the gradient joints. These results demonstrate that DA-based materials present a promising platform for constructing complex yet mechanically robust materials with broadly varied mechanical properties. This result sets the path for the development of additively manufactured polymer parts with gradients in strength and elastic modulus.

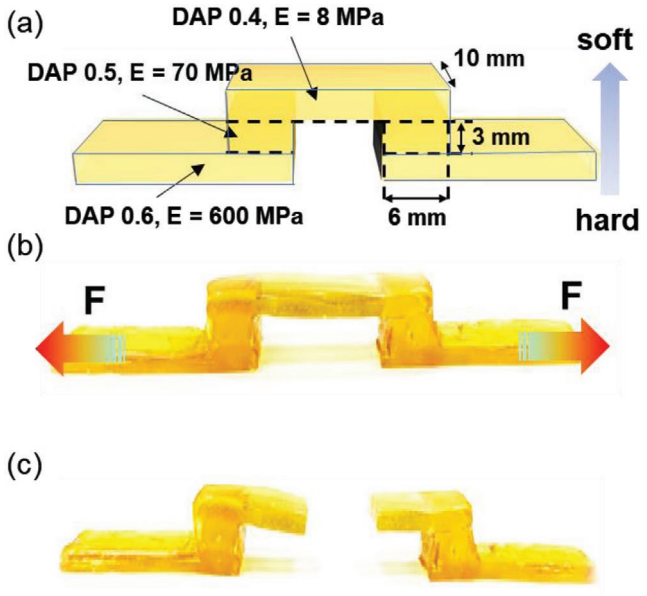

Figure 4. a) Schematic representation of a bridge object design and b) actual 3D-printed object constructed with mechanically mismatched DAP 0.4, 0.5, and 0.6 for tensile testing; c) the bridge object fractured at the center of the top section during tensile testing, showing strong bonding at the mismatched interfaces.

It was reasonable to suggest that the DA reaction could not only support good interbonding of 3D printed DAP materials, but also facilitate self-healing after mechanical damage. The role of dynamic covalent bonds in self-healing has been exploited previously. However, in most cases, a significant degree of healing could only be attained after application of external triggers such as heat, light, or the addition of a healing agent.[28] Indeed, examples of autonomous self-healing in bulk polymers under ambient conditions are rare.[15,28a,29] In contrast to these prior reports, this work shows that the elastomeric DAP 0.4 (T_g < room temperature) demonstrated a remarkable self-healing behavior at room temperature, with the fractured surfaces being able to interconnect by simply bringing them into contact (with no additional applied pressure other than the light human-applied pressure experienced when placing the two surfaces together) and holding for 10 s, as illustrated in **Figure 5**a. The trace of the fracture surfaces disappeared within 12 h at room temperature (Figure S7, Supporting Information). We suggest that the fast healing behavior in this material results from high flexibility of polymer chains, which enables the DA-carrying functional groups to diffuse toward one another and reconnect via the "click" DA reaction. The rupture of the interface most likely occurred through breaking the DA adduct in which the energy of C–C σ-bonds of 96.2 kJ mol^{-1} is more than threefold lower than that of a typical covalent bond energy of a single C–C bond of 348 kJ mol^{-1}.[9b,12a,14] Because of the mismatch in the bond energies, it can be assumed that the failure originates from the breakage of DA bonds and results in generation of furan and maleimide groups, which then react upon contact of the fractured surfaces.[12a,f]

To investigate the healing efficiency of DAPs, tensile testing was performed using cast-molded DAP specimens. After the initial failure, the fractured surfaces were placed into contact and allowed to heal for 12 h at different temperatures. The healing efficiency was calculated as the percentage of the tensile strength restored after healing.[28c] As shown in Figure 5b, the healing efficiencies of DAP 0.4 at 25, 50, and 75 °C were 80%, 93%, and 96%, respectively. DAP 0.6 did not heal at 25 °C but its healing efficiency at 50 and 75 °C was 60% and 80%, respectively. While the DAP 0.6 samples did show healing ability, the healing efficiency was significantly lower compared to those of the less crosslinked DAP networks (DAP 0.4) (Figure 5b). Since the glass transition temperature of a weakly crosslinked DAP 0.4 was as low as 7 °C (Figure 3a), the elastomeric polymer network was able to close the gap between the two fracture surfaces at room temperature, showing high healing efficiency. At the same time, a DAP network with a higher degree of crosslinking (DAP 0.6) having a T_g of 32 °C had limited chain mobility at room temperature and did not heal until the temperature was raised above its T_g. The key factor in the autonomous self-healing behavior was therefore sufficient chain mobility which enabled reformation of dynamic covalent bonds upon contact of the fractured surfaces.[15]

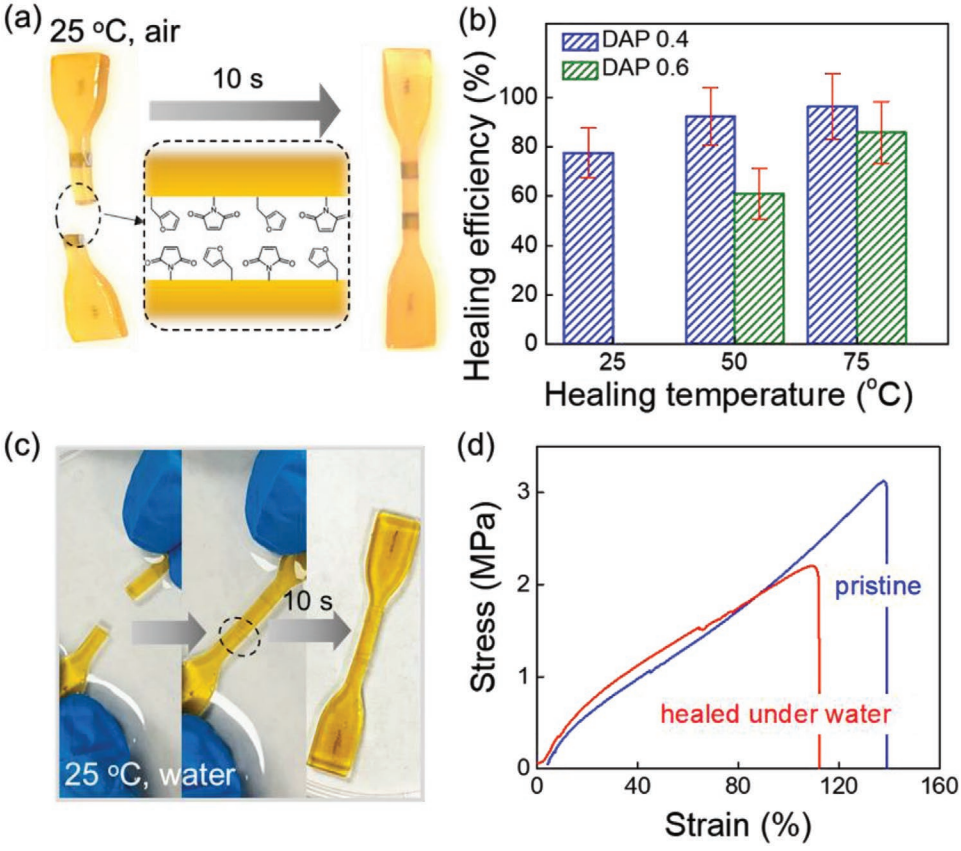

Figure 5. a) Fast mending of fractured surfaces via DA reaction between furan and maleimide groups at the fractured surfaces; b) the healing efficiency of DAP 0.4 and DAP 0.6 healed for 12 h in air at 25, 50, and 75 °C; c) DAP 0.4 specimen demonstrating fast mending of fractured surfaces under water; d) stress–strain curves of the DAP 0.4 specimen before and after underwater healing for 12 h at 25 °C.

Notably, we also found that ruptured surfaces could be mended when the sample was kept under water. When two fractured surfaces were put into contact while immersed in deionized water at room temperature, the surfaces adhered to one another within 10 s (Figure 5c). Figure 5d shows that after 12 h of immersion in water at room temperature, the specimen showed ≈70% recovery of its tensile strength and ≈80% of its strain at break. This behavior is enabled by the robustness of the DA reaction, which can be even accelerated in the presence of water.[30] Previously, self-healing under water was only achieved utilizing either noncovalent interactions, such as hydrogen bonding, or ionic interactions.[13,31] Here, we report for the first time, to the best of our knowledge, a covalently crosslinked polymer material that demonstrates room-temperature autonomous self-healing in an aqueous environment. Such a behavior is highly desirable for applications requiring highly moist or wet conditions, such as underwater soft robotics.

Finally, we exploited the role of the two types of DA attachment between maleimide and furan—the thermodynamically favored *exo* adduct and the kinetically favored *endo* adduct (Figure S8, Supporting Information)—in an unusual shape memory behavior of the networks that allows for reprogramming of the permanent shape of an object. Such behavior is based on the solid-state plasticity of the network above the glass transition temperature which can be used for shape morphing by annealing at ≈60–100 °C.[13] Here, we aimed to uncover the molecular mechanism of such transitions and use this knowledge to control shape transformations. **Figure 6**a shows that when DAP 0.4 was prepared by natural cooling from 120 °C to room temperature, the DSC data showed two endothermic peaks at 80 and 119 °C (Figure 6a, the data for zero annealing time). The lower temperature peak is assigned to dissociation of *endo*-attached crosslinkers, which are characterized by ≈2 kcal mol^{-1} higher Gibbs free energy as compared to

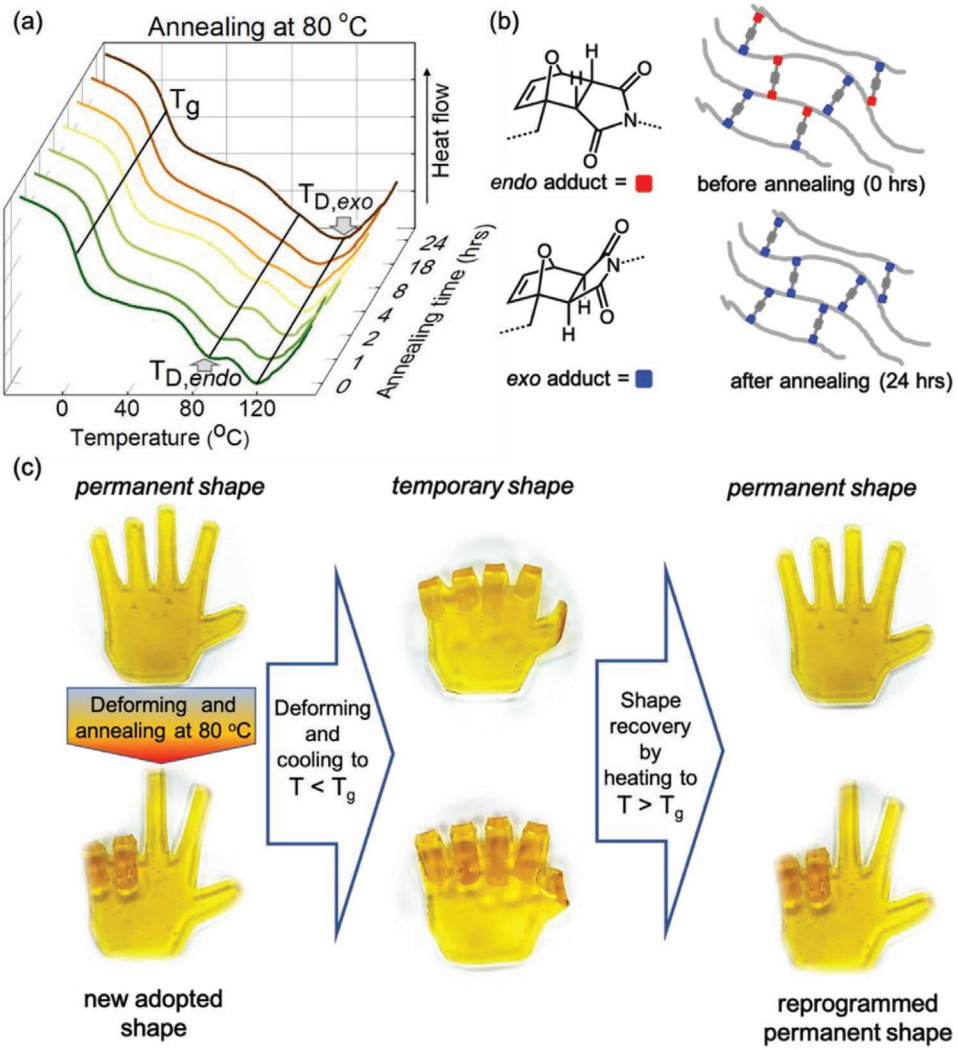

Figure 6. Reprogramming shape-memory behavior of DAP networks. a) Conversion of *endo* to *exo* attachments in the DAP, shown as endothermal peaks with T_D, *endo* = 80 °C and T_D, *exo* = 119 °C, respectively, as a function of annealing time at 80 °C; b) Chemical structures of *endo* and *exo* attachments and schematic representation of DAP networks before and after annealing at 80 °C; c) demonstration of a traditional shape-memory behavior of a 3D-printed hand (top), and rewriting the shape memory of DAP networks through adoption of a new permanent shape via deformation at 80 °C.

exo-attached counterparts.[18b] During cooling, both *endo* and *exo* crosslinking occurred, which persisted within the network until the temperature of dissociation of *endo* adducts, $T_{D,endo}$, of 80 °C. During annealing at 80 °C, the area of the *endo* peak gradually decreased with time, as weaker *endo* attachments of the crosslinks converted to *exo* attachments with a higher dissociation temperature $T_{D,exo}$ (Figures 1b and 6a). During annealing, the rearrangements of a two-type-crosslinker to a one-type-crosslinker network enabled plastic deformation of DAP materials, thus allowing us to alter the shape of the objects without disrupting the integrity of the dynamic network (Figure 6b). Figure 6c illustrates the utilization of such rearrangements for reprogramming the permanent shape of a 3D-printed object (a hand) made of DAP 0.4 resin. Note that the hand could demonstrate the classical shape memory effect following the top route, which includes programming a temporary shape followed by recovery to the initial shape at 30 °C (i.e., at a temperature higher than T_g) . In addition to traditional approach to shape memory behavior, a new permanent shape could be adopted in the material system developed in this work via plastic deformation into a new shape during annealing at 80 °C (the bottom route). Because of the different energies and dissociation temperatures of the *endo* and *exo* attachments, it is reasonable to suggest that the *endo* adducts dissociate at temperatures between $T_{D,endo}$ and $T_{D,exo}$, while the *exo* adducts remain nondissociated during annealing. Therefore, because of the disruption of the *endo* crosslinks in the network, the material was able to accommodate shape changes and "memorize" them as the dissociated DA reactants progressively formed more thermally stable *exo* adducts. As a result, the object recovered to the new permanent shape when heated to 30 °C. While a similar reprogramming of shape memory through plasticity of polymer networks was demonstrated previously,[13] here we point to the underlying mechanism of such behavior. Importantly, we found the DAP network gradually lost the ability for such reprogramming after rewriting the permanent shape memory multiple times during which the *endo* attachments were gradually converted into *exo* attachments (Figure S9, Supporting Information, each rewriting involved 8 h annealing at 80 °C). This suggests the presence of the *endo* attachments in the network was required for such a shape memory effect.

3. Conclusions

In summary, we have reported a family of 3D printable dynamic covalent polymer networks with widely variable mechanical properties and self-healing capabilities. These properties are enabled by the robust, reversible DA reaction between maleimide and furan functionalities on a crosslinker and the prepolymer chains. The materials could be fabricated with "on-demand" mechanical characteristics ranging from soft elastomers to rigid thermosets using a facile solvent-free LDM technique using liquid resins with the same rheological characteristics. Importantly, as-printed objects demonstrated tensile strength similar to that of the molded counterparts, and could be reprinted at least three times with no degradation in their mechanical performance. The proposed family of liquid polymers enabled printing of strongly interbonded, mechanically heterogeneous objects, which showed no preferential damage at multimaterial interfaces under tensile deformation. The robustness of the DA reaction and crosslinking-controlled flexibility of the network chains enabled achieving elastomeric materials which exhibit autonomous healing at room temperature both in air and under water. Finally, our finding of *endo*-to-*exo* isomerization and rearrangement of the network during solid-state annealing allowed altering and reprogramming of the permanent shape of the objects in the solid state without the need of liquefying these materials. The proposed materials platform is a powerful means for fabrication of mechanically diverse objects with tunable self-healing and reprogrammable shape memory behavior via facile 3D printing techniques.

4. Experimental Section

Materials and Polymer Synthesis: Neopentyl glycol diglycidyl ether (NGDE) and furfurylamine (FA) were purchased from Sigma Aldrich and were used as received. BMI was purchased from Sigma Aldrich and was crystallized from dimethylformamide (DMF) before using.

The linear prepolymer was synthesized via ring opening polymerization of the epoxide monomer, NGDE, with FA (Figure S1, Supporting Information). The epoxy equivalent of NGDE was determined as 148 g mol^{-1} by titration with hydrobromic acid. NGDE and FA were added at a 1.9 epoxide/amine ratio. The mixture was heated to 70 °C in 1 h, and the reaction was carried out under continuous stirring under argon at 70 °C for 15 h. After completion of the reaction, a light yellow viscous liquid was obtained. The weight average molecular weight (M_w) of the resulting linear prepolymer was 7000 g mol^{-1}, the polydispersity index was 1.4 as determined by GPC (Figure S2, Supporting Information), and the glass transition temperature was –10.6 °C (Figure S3, Supporting Information).

DAPs were prepared by crosslinking between the linear prepolymer with BMI crosslinker. Briefly, various amounts of BMI crosslinker, calculated to achieve desired maleimide/furan ratios Φ_{BMI}, were dissolved into the linear prepolymer at 120 °C. The BMI/prepolymer melts were cooled down to room temperature naturally to obtain DAP networks with varied crosslinking densities. Fourier transform infrared (FTIR) spectra of the DAP 0.4, the linear prepolymer, and NGDE monomer are shown in Figure S10 (Supporting Information).

3D Printing: Samples were additively manufactured by using a Makerbot Replicator 2X in which a syringe-based extruder was incorporated based on the custom design developed by Hinton et al.[32] The modification allows for the rotary motion of the original stepper motors from the thermoplastic extruder to be converted to linear motion to drive the syringe plunger. By using the original stepper motors, the syringe extruder can be controlled by the same software included in the printer. Aside from changing print parameter settings and start/stop conditions, software modifications were unnecessary. The printing was performed at a nozzle (and syringe) temperature of 120 °C. The base plate temperature was kept at 25 °C. Other printing parameters included a printing speed of 15 mm s^{-1}, a fixed layer height of 0.3 mm, and a solid infill of 100%. A linear print pattern was used with an alternating 45° print direction. For 3D printing of layered heterogeneous objects, each layer was constructed using the same printing parameters given earlier. Different identical syringes were used for printing of each consecutive layer. After a layer of a respective DAP was completed, printing was paused and the syringe containing a different DAP swapped. The printing of a consecutive layer was then resumed.

Materials Characterization Techniques FTIR: FTIR spectroscopy measurements (Bruker, Tensor II) were employed to confirm chemical compositions of the prepolymer and DAP networks. Liquid monomers, linear prepolymer, and crosslinked DAP powders were characterized by attenuated total reflectance (ATR) mode with a high-pressure

clamp attachment. The spectra were recorded from 4000 to 600 cm^{-1}, with resolution of 4 cm^{-1}.

Gel Permeation Chromatography: GPC analysis of linear prepolymers was conducted at 40 °C using a GPC (Agilent) system equipped with a Phenogel 5 µm column. DMF was used as an eluent with a flow rate of 0.2 mL min^{-1}, and the system was calibrated using DMF solutions of poly(ethylene oxide) standard samples (American Polymer Standards Corporation).

^{13}C NMR: The ^{13}C cross polarization magic-angle spinning (CP MAS) NMR experiments were carried out with a Bruker Avance-400 solid-state NMR spectrometer equipped with a standard three-channel 4 mm MAS probe head. The standard proton-carbon CP pulse sequence was applied for spinning samples at a spinning rate of 10 kHz at a contact time of 1.6 ms and a 900 1H pulse of 4.5 µs. The external standard used for solid-state NMR was a tetramethylsilane (TMS) solution.

Rheology Analysis: The rheological measurements were performed using a TA Instruments DHR-2 Rheometer equipped with parallel plate grippers of 40 mm in diameter, and the gap distance was set at 1 mm. Viscosity measurements were carried out with temperature ramped from 140 to 100 °C, $\omega = 10$ rad s^{-1}. Oscillatory temperature sweeps were implemented from 70 to 120 °C at a rate of 2.5 °C min^{-1} with $\omega = 10$ rad s^{-1}.

Thermal Analysis: The glass transition temperature (T_g) and retro DA reaction temperature (T_D) of the linear prepolymer (T_g only) and crosslinked DAPs were determined via DSC. The samples were prepared by weighing ≈10 mg of material into T_{zero} aluminum pans, which were then hermetically sealed. The data were recorded using a TA Instrument DSC 2500. The experiments were conducted at 5 °C min^{-1} temperature ramp from −50 to 140 °C under constant nitrogen gas flow of 50 mL min^{-1}.

Mechanical Testing: Mechanical tensile testing of dogbones (following ASTM D638) was performed using an MTS tensile test frame. Testing was performed at a displacement rate of 10 mm min^{-1} (a strain rate of 0.8 min^{-1}) at room temperature. Displacement was measured using a laser extensometer. The elastic modulus was taken as the initial 0.5% linear portion of the stress–strain curve. The ultimate tensile strength and elongation at break were recorded at material failure. Values reported represent engineering stresses and strains (normalized by initial geometric dimensions).

Optical Microscopy Imaging: A Zeiss Axiovert 200 optical microscope equipped with an AxioCam DCC camera (Zeiss) was used to monitor the healing process of the fractured surfaces within a DAP 0.4 and DAP 0.5 films (≈0.6 mm thickness) at room temperature. The films were cut by a razor blade. The initial length of the cut was ≈3 mm. The cut was closed by aligning the fractured surfaces and putting them into contact. The cut region was then monitored under the optical microscope; images were taken at certain time intervals to record the healing process.

Supporting Information

Supporting Information is available from the Wiley Online Library or from the author.

Acknowledgements

The authors acknowledge the financial support from U.S. Combat Capabilities Development Command Army Research Laboratory under Cooperative Agreement Nos. W911NF-16-2-0229, W911NF-18-2-0232, and W911NF-19-2-0264. Use of the TAMU Materials Characterization Facility, the TAMU Soft Matter Facility, and the Nuclear Magnetic Resonance Facility in the Department of Chemistry is acknowledged.

Conflict of Interest

The authors declare no conflict of interest.

Keywords

3D printing, dynamic covalent polymer network, reprocessable crosslinked polymers, self-healing materials, shape memory polymers

Received: March 13, 2020
Revised: April 9, 2020
Published online: May 19, 2020

[1] W. Yang, V. R. Sherman, B. Gludovatz, E. Schaible, P. Stewart, R. O. Ritchie, M. A. Meyers, *Nat. Commun.* **2015**, *6*, 6649.
[2] a) C. Sanchez, H. Arribart, M. M. G. Guille, *Nat. Mater.* **2005**, *4*, 277; b) H. Qin, T. Zhang, N. Li, H.-P. Cong, S.-H. Yu, *Nat. Commun.* **2019**, *10*, 2202.
[3] a) K. U. Claussen, T. Scheibel, H. W. Schmidt, R. Giesa, *Macromol. Mater. Eng.* **2012**, *297*, 938; b) N. Naserifar, P. R. LeDuc, G. K. Fedder, *Adv. Mater.* **2016**, *28*, 3584.
[4] a) D. Kokkinis, F. Bouville, A. R. Studart, *Adv. Mater.* **2018**, *30*, 1705808; b) J. O. Hardin, T. J. Ober, A. D. Valentine, J. A. Lewis, *Adv. Mater.* **2015**, *27*, 3279; c) M. A. Skylar-Scott, J. Mueller, C. W. Visser, J. A. Lewis, *Nature* **2019**, *575*, 330.
[5] J. J. Senior, M. E. Cooke, L. M. Grover, A. M. Smith, *Adv. Funct. Mater.* **2019**, *29*, 1904845.
[6] a) J. Lee, A. R. Unnithan, C. H. Park, C. S. Kim, in *Biomimetic Nanoengineered Materials for Advanced Drug Delivery* (Eds: A. R. Unnithan, A. R. K. Sasikala, C. H. Park, C. S. Kim), Elsevier, Amsterdam **2019**, p. 61; b) T. N. A. T. Rahim, A. M. Abdullah, H. Md Akil, *Polym. Rev.* **2019**, *59*, 589.
[7] C. Weller, R. Kleer, F. T. Piller, *Int. J. Prod. Econ.* **2015**, *164*, 43.
[8] M. Nadgorny, A. Ameli, *ACS Appl. Mater. Interfaces* **2018**, *10*, 17489.
[9] a) A. Gandini, *Prog. Polym. Sci.* **2013**, *38*, 1; b) M. A. Tasdelen, *Polym. Chem.* **2011**, *2*, 2133.
[10] Y.-L. Liu, T.-W. Chuo, *Polym. Chem.* **2013**, *4*, 2194.
[11] a) G. Zhang, Q. Zhao, L. Yang, W. Zou, X. Xi, T. Xie, *ACS Macro Lett.* **2016**, *5*, 805; b) J.-M. Raquez, S. Vanderstappen, F. Meyer, P. Verge, M. Alexandre, J.-M. Thomassin, C. Jérôme, P. Dubois, *Chem. - Eur. J.* **2011**, *17*, 10135.
[12] a) X. Chen, M. A. Dam, K. Ono, A. Mal, H. Shen, S. R. Nutt, K. Sheran, F. Wudl, *Science* **2002**, *295*, 1698; b) Q. Tian, Y. C. Yuan, M. Z. Rong, M. Q. Zhang, *J. Mater. Chem.* **2009**, *19*, 1289; c) M. Fan, J. Liu, X. Li, J. Zhang, J. Cheng, *Ind. Eng. Chem. Res.* **2014**, *53*, 16156; d) W. Zou, J. Dong, Y. Luo, Q. Zhao, T. Xie, *Adv. Mater.* **2017**, *29*, 1606100; e) J. Ax, G. Wenz, *Macromol. Chem. Phys.* **2012**, *213*, 182; f) X. Chen, F. Wudl, A. K. Mal, H. Shen, S. R. Nutt, *Macromolecules* **2003**, *36*, 1802; g) Y.-L. Liu, C.-Y. Hsieh, *J. Polym. Sci., Part A: Polym. Chem.* **2006**, *44*, 905; h) A. A. Kavitha, N. K. Singha, *J. Polym. Sci., Part A: Polym. Chem.* **2007**, *45*, 4441; i) K. C. Koehler, D. L. Alge, K. S. Anseth, C. N. Bowman, *Biomaterials* **2013**, *34*, 4150.
[13] N. N. Xia, X. M. Xiong, J. Wang, M. Z. Rong, M. Q. Zhang, *Chem. Sci.* **2016**, *7*, 2736.
[14] A. Sanyal, *Macromol. Chem. Phys.* **2010**, *211*, 1417.
[15] M. M. Diaz, J. Brancart, G. Van Assche, B. Van Mele, *Polymer* **2018**, *153*, 453.
[16] K. Yang, J. C. Grant, P. Lamey, A. Joshi-Imre, B. R. Lund, R. A. Smaldone, W. Voit, *Adv. Funct. Mater.* **2017**, *27*, 11.
[17] J. Herzberger, J. M. Sirrine, C. B. Williams, T. E. Long, *Prog. Polym. Sci.* **2019**, *97*, 101144.
[18] a) J. Carneiro de Oliveira, M.-P. Laborie, V. Roucoules, *Molecules* **2020**, *25*, 243; b) L. Rulíšek, P. Šebek, Z. Havlas, R. Hrabal, P. Čapek, A. Svatoš, *J. Org. Chem.* **2005**, *70*, 6295.
[19] B. J. Adzima, H. A. Aguirre, C. J. Kloxin, T. F. Scott, C. N. Bowman, *Macromolecules* **2008**, *41*, 9112.

[20] S. Vinayagamoorthi, C. T. Vijayakumar, S. Alam, S. Nanjundan, *Eur. Polym. J.* **2009**, *45*, 1217.
[21] a) B. S. Chiou, S. R. Raghavan, S. K. Khan, *Macromolecules* **2001**, *34*, 4526; b) Q. Q. Dou, A. Karim, X. J. Loh, *Polymers* **2016**, *8*, 341; c) P. Karimineghlani, E. Emmons, M. J. Green, P. Shamberger, S. A. Sukhishvili, *J. Mater. Chem. A* **2017**, *5*, 12474; d) P. Karimineghlani, A. Palanisamy, S. A. Sukhishvili, *ACS Appl. Mater. Interfaces* **2018**, *10*, 14786.
[22] R. Gheneim, C. Perez-Berumen, A. Gandini, *Macromolecules* **2002**, *35*, 7246.
[23] a) V. D. Kiselev, D. A. Kornilov, I. A. Sedov, A. I. Konovalov, *Int. J. Chem. Kinet.* **2017**, *49*, 61; b) S.-Y. Tang, J. Shi, Q.-X. Guo, *Org. Biomol. Chem.* **2012**, *10*, 2673.
[24] J. R. Davidson, G. A. Appuhamillage, C. M. Thompson, W. Voit, R. A. Smaldone, *ACS Appl. Mater. Interfaces* **2016**, *8*, 16961.
[25] D. Yuan, H. Guo, K. Ke, I. Manas-Zloczower, *Composites, Part A* **2020**, *132*, 105837.
[26] T. Kamon, H. Furukawa, *Epoxy Resins and Composites IV*, Advances in Polymer Science, Vol. *80*, Springer, Berlin **1986**, p. 173.
[27] a) D. J. Jiao, F. Lossada, W. Q. Yu, J. Q. Guo, D. Hoenders, A. Walther, *Adv. Funct. Mater.* **2019**, 1905309; b) R. Libanori, R. M. Erb, A. Reiser, H. Le Ferrand, M. J. Suess, R. Spolenak, A. R. Studart, *Nat. Commun.* **2012**, *3*, 1265.
[28] a) P. A. Pratama, M. Sharifi, A. M. Peterson, G. R. Palmese, *ACS Appl. Mater. Interfaces* **2013**, *5*, 12425; b) B. R. Zhang, J. Ke, J. R. Vakil, S. C. Cummings, Z. A. Digby, J. L. Sparks, Z. J. Ye, M. B. Zanjani, D. Konkolewicz, *Polym. Chem.* **2019**, *10*, 6290; c) Y. Heo, H. A. Sodano, *Adv. Funct. Mater.* **2014**, *24*, 5261.
[29] J. J. Cash, T. Kubo, A. P. Bapat, B. S. Sumerlin, *Macromolecules* **2015**, *48*, 2098.
[30] R. Breslow, T. Guo, *J. Am. Chem. Soc.* **1988**, *110*, 5613.
[31] a) W.-P. Chen, D.-Z. Hao, W.-J. Hao, X.-L. Guo, L. Jiang, *ACS Appl. Mater. Interfaces* **2018**, *10*, 1258; b) B. K. Ahn, D. W. Lee, J. N. Israelachvili, J. H. Waite, *Nat. Mater.* **2014**, *13*, 867.
[32] T. J. Hinton, Q. Jallerat, R. N. Palchesko, J. H. Park, M. S. Grodzicki, H.-J. Shue, M. H. Ramadan, A. R. Hudson, A. W. Feinberg, *Sci. Adv.* **2015**, *1*, e1500758.